Quantum jumps in the PEMFC science and technology from the 1960s to the year 2000
Part II. Engineering, technology development and application aspects ☆

Paola Costamagna[*], Supramaniam Srinivasan

Center for Energy and Environmental Studies, Princeton University, Princeton, NJ 08544-5263, USA

Abstract

The technology of proton exchange membrane fuel cells (PEMFCs) has now reached the test-phase, and engineering development and optimization are vital in order to achieve to the next step of the evolution, i.e. the realization of commercial units. This paper highlights the most important technological progresses in the areas of (i) water and thermal management, (ii) scale-up from single cells to cell stacks, (iii) bipolar plates and flow fields, and (iv) fuel processing. Modeling is another aspect of the technological development, since modeling studies have significantly contributed to the understanding of the physico-chemical phenomena occurring in a fuel cell, and also have provided a valuable tool for the optimization of structure, geometry and operating conditions of fuel cells and stacks. The 'quantum jumps' in this field are reviewed, starting from the studies at the electrode level up to the stack and system size, with particular emphasis on (i) the 'cluster–network' model of perfluorosulfonic membranes, and the percolative dependence of the membrane proton conductivity on its water content, (ii) the models of charge and mass transport coupled to electrochemical reaction in the electrodes, and (iii) the models of water transport trough the membrane, which have been usefully applied for the optimization of water management of PEMFCs. The evolution of PEMFC applications is discussed as well, starting from the NASA's Gemini Space Flights to the latest developments of fuel cell vehicles, including the evolutions in the areas of portable power sources and residential and building applications. © 2001 Elsevier Science B.V. All rights reserved.

Keywords: Proton exchange membrane fuel cells; Water and thermal management; Fuel processing; Modeling

1. Quantum jumps in PEMFC engineering leading to rapid technology development

Proton exchange membrane fuel cells (PEMFCs) have reached the test and demonstration phase, and an impressive research effort has been made in order to reach this stage of development. While Part I of this review focuses on the 'quantum jumps' in the fundamental scientific areas made so far, Part II deals with the engineering and technology development. The paper is structured as follows: the first part (quantum jumps in PEMFC engineering leading to rapid technology development) discusses the evolution of cells and components, with particular attention to the fuel processing issues and with particular emphasis on modeling; the second part (quantum jumps in technology development and applications) focuses on the applications and finally the third section (technological and economic challenges and 21st century perspectives) discusses the technical and economic challenges still faced with for reaching the era of applications and commercialization in the 21st century.

1.1. Single cell and cell stacks

1.1.1. Bipolar plates and flow fields

Bipolar plates supply the reactant gases through the flow channels to the electrodes and serve the purpose of electronically connecting one cell to another in the electrochemical cell stack. The essential requirements, in respect to physico-chemical characteristics, are high values of electronic conductivity, high mechanical strength, impermeability to reactant gases, resistance to corrosion and low cost of automated production. Gold coated titanium and niobium were the materials used by General Electric in the 1960s, and in

the early 1970s they were substituted by graphite, as in the PAFC technology, because of its high corrosion resistance and low cost. Graphite bipolar plates are manufactured starting from high surface area graphitic carbon powder mixed with ligand resins; after molding at high temperature and pressure, the gas distribution channels are machined into the graphite blocks. The gas channels are machined into the graphite bipolar plates, generally in a parallel flow configuration. Fuel cell developers have used alternative designs, such as (i) series-parallel flow (IFC, Energy Partners), (ii) serpentine (Ballard), (iii) interdigitated flow and (iv) flow through porous carbon or stainless steel (IFC, De Nora). Due to the small pressure drop between the inlet and outlet ports, there are no water droplet blockages in the bipolar plates with serpentine flow geometry, as used in the Ballard PEMFCs. The interdigitated flow field [1] is attracting a wide interest at the present time. In this case, the reactant gases are forced to flow into the active layer of the electrodes, where the forced convection (instead of diffusion) avoids flooding and gas diffusion limitations, thereby extending the linear region of the cell potential versus current density plot [2]. Flow-through porous carbon [3] has also been proposed for improved water management; a better method may be the use of flow-through porous metallic meshes (with high resistance to corrosion), to improve gas distribution on the cell plane [4]. Due to the high cost of production, in spite of the automated machining of the channels, alternative materials have been explored, e.g. coated metals and alloys [5] (e.g. gold coated aluminum and stainless steel), titanium, exfoliated graphite [5], Fe-based alloys [6] and conducting plastics. Such materials could be stamped, thereby lowering the costs of production of the bipolar plates; however, corrosion and lifetime issues have not been solved at present.

1.1.2. Water management

Proton conduction in sulfonic acid membranes is due to proton hopping from one sulfonic group to another (Grotthus mechanism). In the presence of water, both the proton and the sulfonic groups are in the solvated form, and this greatly facilitates the hopping mechanism (specific conductivity of about 0.1 S/cm for a fully hydrated Nafion® membrane at 80°C). Thus, the maximum degree of hydration of the membrane electrolyte is vital for the PEMFC to attain its highest performance; otherwise, the ohmic overpotential in the membrane could be a major source of loss of efficiency in the PEMFCs. In the 1960s, when polystyrene sulfonic acid membranes were used in the General Electric fuel cells, which were operated at low power densities (<100 mA/cm^2), the product water was sufficient to keep the electrolyte wet via a wicking mechanism. In the 1970s, with the 'quantum jump' due to the invention of Nafion®, various humidification strategies have proposed to fulfill the higher water retention characteristics of the membrane. The humidification system proposed at that time, which is still the state-of-the-art, consists of humidifying the reactant gases with

liquid water; if the residence time is long enough, the gases will then be almost 100% humidified. The temperature of the humidification bottles is an important parameter, and optimization studies carried out during the 1980s have established that the humidification temperature has to be higher than that of the fuel cell (5°C for the oxygen or air and 10°C for hydrogen) [7]. Alternative techniques have been proposed during the years, such as (i) recirculation of the exhaust flows, (ii) water vapor injection, consisting of addition of water vapor along the gas flow channels, (iii) liquid water injection [8], consisting of addition of water droplets into the inlet gaseous streams and (iv) use of wicks to connect the polymeric electrolyte to an external water reservoir [9]. All these methods lead to good cell performance, and this is particularly true with techniques (iii) and (iv), where the membrane is humidified through liquid instead of vapor water. Technique (iii) has the additional advantage that there is no need for heating the humidification section, and evaporation of the liquid droplets saturates the reactant streams as well as facilitates efficient thermal management system. The problem of electrode flooding which arises in cells with parallel flow is overcome when this method is applied to interdigitated flow fields [2], thanks to the forced convection regimen into the active layers of the electrodes.

In the 1990s, the potential applications of PEMFCs for electric vehicles have stimulated the development of internal hydration techniques, where the water produced by the electrochemical reaction is used for the hydration of the membrane, allowing the elimination of an external humidification sub-system: this method can also reduce the volume and weight and thus the size of the overall system. Several methods have been proposed, such as (i) use of porous carbon blocks for the bipolar plates, which, thanks to capillary condensation, are able to retain the water produced by the electrochemical reaction and also assist water transport from the cathodic to the anodic side of the fuel cell. In this type of cell stack, the carbon blocks are not channeled, and the gases are humidified by forcing them to flow through the wet porosities [3], (ii) impregnation of the membrane solution into the electrode, forming a thin recast film on the surface, followed by hot-pressing of two impregnated electrodes onto each other. By this procedure, very thin electrolyte films can be prepared, which show very small ohmic resistance and thus allow operation even under unfavorable conditions, such as low pressure and temperature and without external humidification [10] and (iii) impregnation of thin Nafion recast membranes with a small amount (around 5–6 wt.%) of nanosize Pt particles. In this case, Pt catalyzes the production of water from the cross-over flux of H_2 and O_2 across the membrane, thereby ensuring a satisfactory hydration level [11].

1.1.3. Scale-up issues and thermal management

PEMFCs, unlike other types of fuel cells, show some loss of efficiency and power density with the scale-up of areas of

electrodes and increase in number of cells in a stack. The main reason is that removal of the product, liquid water, becomes more difficult in larger systems; furthermore, a high water vapor pressure in the reactant flows causes an increase in overpotential, especially at the cathode [12]. In addition, water condensation, electrode flooding and occlusion of the gas channels can occur, leading to operational failure. Methods like cyclic and rapid ejection of the excess water through purge valves, which have been evaluated, do not satisfactorily solve this problem. A reasonable 'quantum jump' was made by Ballard in the 1990s by using a method which involves at least partial removal of water from the anode side; in this case, liquid water accumulated at the cathode is drawn to the anode by a concentration gradient across the membrane, and removed by the exit gas from the anode in the gaseous phase, by optimizing the extent of humidification and the flow rate of the fuel entering the cell [12,13]. An issue strongly related to water management, is that of thermal management in stacks: on one hand, too low temperatures cause water condensation problems as discussed above, but on the other hand, even more important, is that high cell temperature (even in confined areas) leads to membrane dehydration and consequent loss of performance, as discussed in Section 1.3.3. The 'rule of thumb' for the evaluation of heat losses in PEMFCs is that the power dissipated as heat is approximately equal to the electrical power supplied to the external circuit (deviations from this simple rule take place at very high current density and low voltage [14]). As the temperature difference between the cell and the surroundings is only about 50°C, it is impossible to rely on natural convection and air cooling for efficient heat removal [14]. Water cooling is the only alternative [15], currently used in the state-of-the-art PEMFCs, involving circulation of water through flow channels in cooling plates adjacent to the bipolar plates [16]. Methods for simultaneous water and thermal management in stacks have been proposed, such as liquid water injection (see previous sections) and air plus evaporative cooling [14]. In the latter case, the stack contains a few chambers where the dry cathodic reactant is brought into contact with water; as a result, humidification of the gas and evaporative cooling of water occurs simultaneously. It has been shown that this method appears feasible with air; with pure oxygen it has the disadvantage of requiring too high stoichiometric flowrates.

1.2. Fuel processing

Hydrogen is the ideal fuel for PEMFCs as it yields the highest levels of fuel cell performance, but it is a secondary fuel which has to be produced from primary fuels (natural gas, petroleum or coal), or by electrolysis of water. The near term options for production and delivery of hydrogen include [17] (i) centralized production in large steam-reforming plants, or as a by-product from chemical industries (e.g. chloro-alkali), and truck or pipeline delivery and (ii) hydrogen production and distribution through a network of on-site natural gas reformers or water electrolyzers. In the longer term, hydrogen production from biomass, coal or municipal solid waste, or electrolysis powered by alternative power sources (wind, solar or nuclear) are under serious consideration. For vehicle applications, hydrogen can be stored on-board as a compressed gas, as a cryogenically cooled liquid or as a metal hydride. In the framework of the studies on vehicle applications developed in the 1990s, investigations of on-board production of hydrogen from hydrocarbon and alcoholic liquid fuels such as gasoline and methanol, respectively [18–21], have been stimulated because of the difficulty of on-board storage of hydrogen, safety issues and the immediate unavailability of a hydrogen distribution network proposed in (i) or (ii) above. These liquid fuels are the best choice for vehicles as they have a high energy density and are considerably safer to be carried on-board than compressed gaseous fuels; also, the existing excellent distribution network for gasoline could economically be converted to one for methanol, which can more easily be processed on-board to produce hydrogen. On-board reforming and partial oxidation fuel processors are being developed (Fig. 1); in the former, methanol is the fuel, and the first step involves its reaction with steam at 200–350°C, using copper as the catalyst, to produce H_2, CO_2 and CO. This step is endothermic, and the required heat is supplied to the reactor by the fuel cell exhausts gases. In case of gasoline, the first step of partial oxidation of the fuel occurs at 600–800°C; the reaction is uncatalyzed and it is slightly exothermic. In order to maximize the conversion to H_2 and minimize the CO content, the first step is followed by other conversion steps, which require additional, complicated and expensive reactors. This is realized through high temperature and low temperature catalytic shift converters followed by preferential oxidation (PROX). The first converter takes advantage of the fast kinetics of the shift reaction at high temperature (about 450°C) for reducing the CO concentration to <10%, while the second, because of the thermodynamic equilibrium being favorably shifted at lower temperatures, allows a further reduction of CO to the 1% level. This amount of CO is much above the acceptable threshold for PEMFC applications; thus, a preferential oxidation step follows, where the reformate gas is mixed with a small amount of
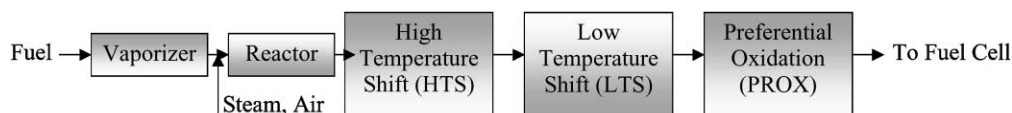

Fig. 1. Schematic of on-board fuel processor.

air and then passed through a packed column of 0.5% Pt on alumina. After this step, the residual CO is about 50 ppm in case of methanol steam-reforming and 100 ppm in case of gasoline partial oxidation. An alternative technology for complete removal of CO has been proposed, e.g. CO filtration through a Pd or Pd-alloy membrane [21]. This technology is less used, in spite of its high efficiency and selectivity, because it has the drawbacks of high costs and need for high pressure differentials across the filtration unit.

Economic evaluations have been carried out in the late 1990s to compare on-board fuel-processing to on-board hydrogen storage. A comparison of the two methods for fuel cell powered electric vehicles [19] shows that the costs are similar in both cases, as the prices of the hydrogen tank and of the fuel processor are comparable. However, it is projected that the two types of cars will exhibit different performances, because (i) the efficiency of the vehicle with pure hydrogen will be higher than that with the reformed fuel, and (ii) the weight and the volume of the reformer-based system will be considerably higher. A techno-economic assessment [17] of fuel cell cars based on compressed hydrogen, methanol steam-reforming and gasoline partial oxidation system revealed that the methanol and the gasoline vehicles will be US$ 500–600 and 850–1200 more expensive than the hydrogen car, respectively. However, if the capital cost for developing a hydrogen and methanol distribution network is taken into consideration, there is again a substantial equivalence.

1.3. Modeling studies of PEMFC performance

Parallel to the development of components for single cells and stacks, modeling studies have been conducted to aid in the optimization of composition and structure of electrodes and membrane–electrode assemblies (MEAs), as well as operating conditions, in order to attain high efficiencies and power densities. The major 'quantum jumps' have been achieved in the late 1980s and in the 1990s, and have allowed a better understanding of the physico-chemical phenomena taking place in PEMFCs. These 'quantum jumps' will be discussed below, starting from the membrane and electrode scale-up to the system level; usually, at each level of the study the results of the previous step are taken into account, often in a parametrized form.

1.3.1. Membrane

After the invention of the Du Pont's perfluorosulfonic acid membrane (Nafion®) in the 1970s, several theoretical studies were developed aimed at correlating the proton conductivity of the membrane to the operating variables, such as temperature and water content of the membrane. The basis for all these models is the description of the microscopic structure of the polymer that was proposed in the early 1980s by Gierke and Hsu [22]. In this work, which can indeed be considered as the first 'quantum jump' in the field of membrane modeling, the authors correlated the experimen-

tal data through geometric and phenomenologic relationships for the swelling of the polymer due to the uptake of water and the diffusion coefficient of water in the membrane pores. The correlation of data taken under different operating conditions led to the formulation of a widely accepted description of the polymeric membrane in terms of an inverted micellar structure in which the ion-exchange sites separate from the fluorocarbon backbone thus forming spherical clusters (pores), which are connected by short narrow channels. When the membrane is in the dry form, an average cluster has a radius of about 1.8 nm and it contains about 26 SO_3^- groups distributed on the inner pore surface. In the swollen form the diameter grows up to about 4 nm and the number of fixed SO_3^- groups increase up to $\sim$70. Under these conditions, each pore is filled with about 1000 water molecules and the connecting channels have a diameter and a length of about 1 nm. In the same work, Gierke and Hsu [22] also proposed the use of percolation theory for the correlation of the electrical conductivity with the water content of the membrane. According to this theory, there is a value for the amount of water impregnated in the membrane, below which ion transport is extremely difficult due to a lack of extended pathway. Above and near the threshold, the conductivity σ follows the law

$$\sigma = \sigma_0 (c - c_0)^n \tag{1}$$

where c is the volume fraction of the aqueous phase, c_0 the percolation threshold for the water content in the membrane, n a universal constant which depends on the dimensionality of the system (usually about 1.5 in 3-D systems) and σ_0 a prefactor related to the molecular interactions, and can only be computed from specific miscroscopic models. A comparison between experimental results and percolation theory is reported in Fig. 2, showing an extremely good agreement.

After the seminal work of Gierke and Hsu [22], other investigators have focused their attention on modeling of the microstructure and of the percolative features of ionic conductivity in perfluorosulfonic membranes. As far as the first aspect is concerned, interesting results have been reported by Okada et al. [23], who, again by interpolation of experimental data, were able to demonstrate that around 50% of the water molecules in the membrane are found to be associated with the SO_3^- sites (primary hydration layer) or the protons, and the remaining 50% is semi-free in the pores (secondary, tertiary, etc., hydration layers). Other recent studies propose an interpretation of the percolation properties of proton conductivity as a function of water content using a random network model and the effective medium theories as applied to the pores and channels of the membrane [24]. The theoretical findings have been shown to be in line with experimental observations of the membrane complex impedance.

1.3.2. Electrode

Fig. 3 shows a detailed schematic of a typical PEMFC electrode, which displays three layers: (i) Teflonized
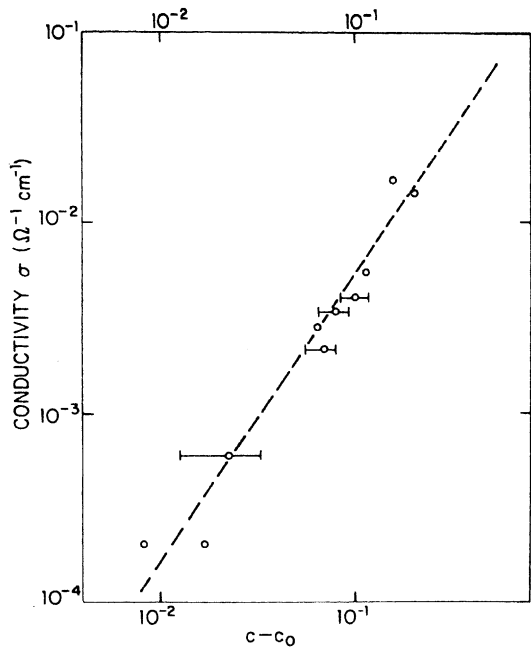
Fig. 2. Log–log plot of Nafion conductivity vs. excess volume fraction $(c - c_0)$ of the aqueous phase. Experimental data measured through a standard ac technique (○): The straight line (− − −) is a least-squares fit of the percolation prediction (Eq. (1)), with $n = 1.5$, $c_0 = 0.1$ and $\sigma_0 = 0.16\ \Omega/\text{cm}$. From [22], with permission.

substrate (typically, carbon cloth); (ii) a diffusion layer, generally formed by carbon particles of about 0.1 μm size along with Teflon and (iii) an active layer, where Pt catalyst grains (dimensions 20–40 Å) are supported on carbon particles (Pt load usually 0.4 mg/cm^2 or less) with or without Teflon; a proton conducting membrane phase partly penetrates the pores in this layer. Even if the void degree is different in the various layers, still a high porosity is characteristic of all the layers of the electrode. Conduction properties differ in the various layers too, as the support and
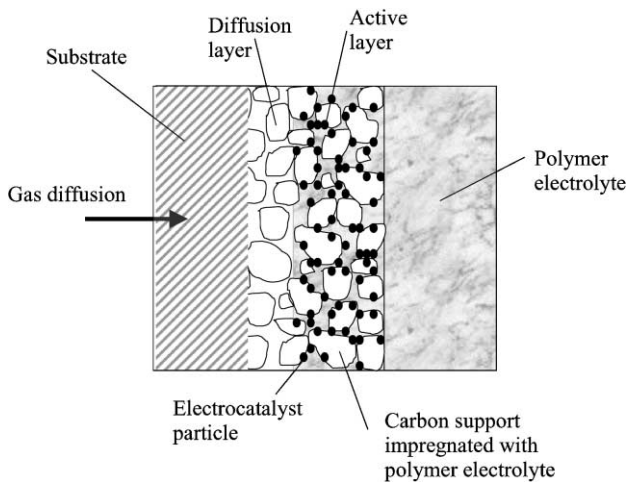

Fig. 3. Schematic of mass and charge transport phenomena in the electrodes.

diffusion layers are electronic conductors, while the active layer, due to the overlapping of electrode and membrane, features two parallel paths for proton and electron conduction (carbon particles and Pt grains form an interconnected electron conducting network through the active layer). Generally, the thickness of the active layer is about 10–100 μm (more recently, closer to the lower end) and the thickness of the overall electrode is 300–400 μm.

The first 'quantum jump' in the electrode simulation was made in the years 1991–1992, when Bernardi et al. [25,26] presented a detailed model for an MEA, which included the analysis of the phenomena occurring in both the membrane and the electrodes. The features of the overall model and the results obtained will be discussed further in a subsequent sub-section; here, we will focus only on the modeling of the electrode. The authors described the relevant processes as (i) gas diffusion, liquid water transport and electron transport through the diffusion layer, (ii) dissolution of oxygen in the polymer-electrolyte phase of the active layer (iii) oxygen diffusion in the polymer-electrolyte phase of the active layer, (iii) charge transfer in the active layer, i.e. proton transfer through the polymer-electrolyte phase and electron transfer through the carbon support and electrocatalyst particles, and (iv) electrochemical reaction in the active layer.

In their study, the authors have not differentiated the substrate from the diffusion layer and considered the membrane to be always fully hydrated; the model is one-dimensional in the direction z perpendicular to the cell plane, and the basic equations are reported as follows: the Stefan–Maxwell equations are used to model the multicomponent diffusion in the porous electrode

$$\nabla x_i = \sum_{j=1}^{n} \frac{RT}{pD_{ij}^{\text{eff}}} (x_i N_{j,g} - x_j N_{i,g}) \tag{2}$$

where n is the number of components of the mixture, $N_{i,g}$ the superficial gas-phase flux of species i averaged over a differential volume element, and the quantity D_{ij}^{eff} is an effective binary diffusivity of the pair i–j in the porous medium. The Butler–Volmer equation is used for the kinetics of the electrochemical reaction

$$j = \frac{di}{dz} = ai_0\{\exp[\alpha_a f(\phi_{\text{solid}} - \phi)] - \exp[-\alpha_c f(\phi_{\text{solid}} - \phi)]\} \tag{3}$$

where j is the transfer current density, i is the current density, a the effective electrocatalyst area per unit volume, i_0 is the exchange current density (mA/cm^2), $f = F/RT$, α_a and α_c are the anodic and cathodic transfer coefficients and ϕ the electrical potential. The exchange current density i_0 is related to the oxygen and proton concentration through the following relationship:

$$i_0 = i_0^{\text{ref}} \left(\frac{c_{O_2}}{c_{O_2}^{\text{ref}}}\right)^{\gamma_{O_2}} \left(\frac{c_{H^+}}{c_{H^+}^{\text{ref}}}\right)^{\gamma_{H^+}} \tag{4}$$

where c is the concentration and γ_{O_2} and γ_{H^+} are phenomenological coefficients. In the active layer, the concentration of oxygen dissolved in the polymeric membrane varies along the z-direction according to the following equation, derived from first Fick's law in combination with the oxygen material balance and the water continuity equation

$$D_{O_2}^{eff} \frac{d^2 c_{O_2}}{dz^2} = v \frac{dc_{O_2}}{dz} + \frac{di}{dz}\left(\frac{s_{O_2}}{n_e F} - \frac{s_w}{n_e F}\frac{c_{O_2}}{\rho}\right) \quad (5)$$

where $D_{O_2}^{eff}$ is the effective diffusion coefficient of oxygen dissolved in the polymeric membrane, s_{O_2} and s_w are stoichiometric coefficients, ρ and v are the density and velocity of liquid water in the membrane pores.

The proton transport in the pores of the membrane in the active layer region is described by an equation derived from the Nernst–Plank expression (see Eq. (8) in Section 1.3.3)

$$-\kappa^{eff}\frac{d\phi}{dz} = i - Fc_f v \quad (6)$$

where κ^{eff}, ϕ and c_f are effective ionic conductivity, the potential and the fixed charge concentration of the membrane respectively. Eq. (6) accounts for both ohmic and convection modes of charge transport through the membranes pores. Also, the movement of the electrons in the solid portion of the catalyst layer is governed by Ohm's law

$$\sigma^{eff}\frac{d\phi_{solid}}{dz} = I + i \quad (7)$$

where σ is the conductivity of the electronically conductive phase and I the cell current density based on the geometric surface area of the electrode.

The scheme of equations reported above has no analytical solution, and thus techniques for numerical integration have been developed. The main results obtained are reported in Figs. 4 and 5. Fig. 4 shows the dissolved oxygen concentration profiles in the membrane portion of the electrocatalyst layer and in the gas diffuser; while the gas diffusion region shows a profile which is almost flat, demonstrating that no gas-diffusion limitations take place in that area; the active
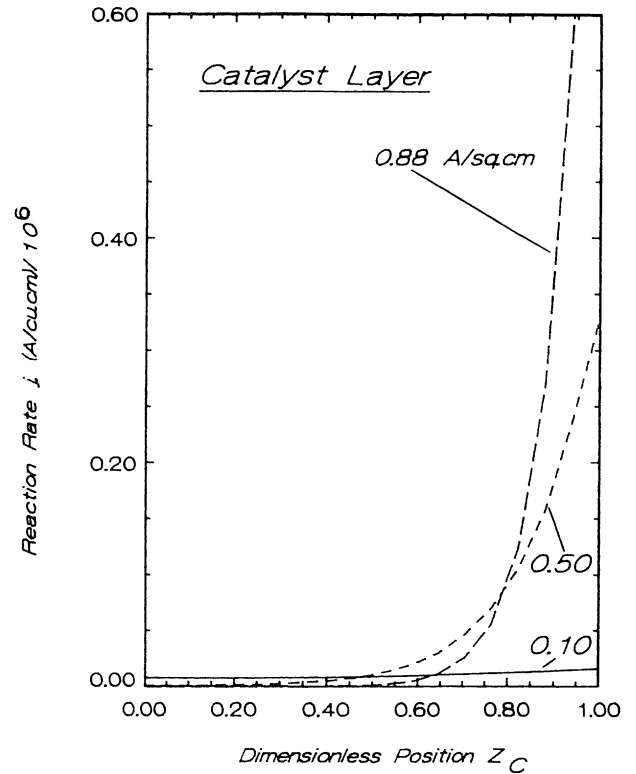

Fig. 5. Model results for spatial variation of reaction rate j throughout active catalyst layer for various current densities. From [25], with permission.

layer region exhibits a different picture. In the active layer, the dissolved oxygen concentration is almost uniform at low current densities, while at high current densities, the portion of the active layer located near to the boundary with the electrolyte is depleted of dissolved oxygen, because the oxygen cannot diffuse fast enough to replenish what is consumed by the electrochemical reaction; however, a limiting current density is not reached until c_{O_2} is 0 in all regions of the electrocatalyst layer. Fig. 5 shows the reaction rate distribution throughout the electrocatalyst layer for the same electrical current densities reported in Fig. 4; as a
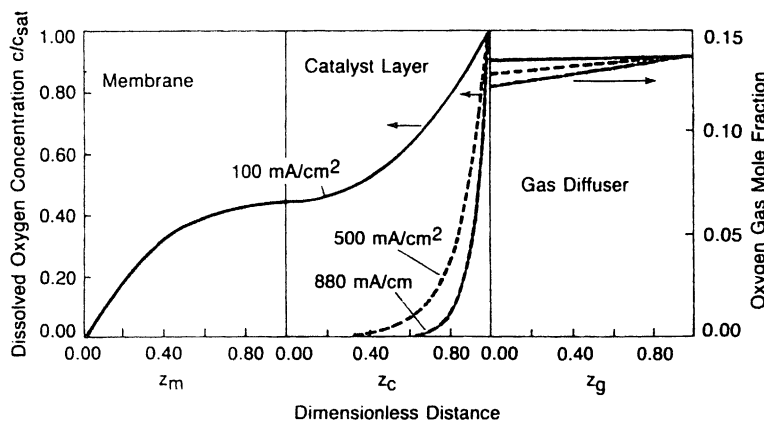

Fig. 4. Model results for spatial variation of dissolved oxygen concentration within the membrane phase of the catalyst layer for various current densities. Adapted from [25], with permission.

consequence of the dissolved oxygen concentration distribution, the reaction rate is almost uniform throughout the catalyst layer only at low current densities (i.e. 100 mA/cm^2); at higher current densities, the current is generated only in a part of the active layer which is close to the interface with the gas diffuser.

Equations similar to the ones discussed above have been applied in different ways in many studies [27–38] aimed at gaining insight on optimization of the electrode composition and structure of the electrode in order to obtain the maximum performance in the PEMFC. In particular, the effects of structural parameters such as polymer volume fraction, catalyst layer thickness and platinum loading in the electrocatalyst layer have been analyzed. The results of the simulations [27,28] show that in case of poor impregnation of the electrolyte into the active layer, the proton conductivity is the limiting electrode process and the current is only generated by a thin layer close to the membrane region; the higher the exchange current density of the electrochemical reaction, the thinner is the region where the charge transfer process occurs. The simulation indicates that there is an optimal value of polymer volume fraction which depends on the electrocatalyst layer thickness, and usually is in the range $\varepsilon = 0.4$–0.5 (where ε is the volume fraction of polymer phase in the catalyst active layer). The optimal value is related to the fact that a trade-off exists between gas diffusion as a controlling factor and ohmic losses becoming important for thicker electrocatalyst layers. In an analogous fashion, the thickness of the active layer has to be chosen on the basis of trade-off considerations, as an increase of the active layer thickness provides a larger active area for the electrochemical reaction, but at the same time mass-transport problems will be encountered at high current densities. Still due to the fact that electrical current is only generated by a thin part of the active layer, an increase of the platinum load in the active layer beyond a certain amount (20 wt.% Pt/ C) would increase the cost, but only slightly improve the performance.

Another 'quantum jump' was made during the years 1993–1998, when the agreement between theory and experimental results was demonstrated by a number of authors [30–32,34,38] (Fig. 6). In particular, some of the studies [29,31,32] have shown that the agglomerate model (i.e. the active layer contains intersecting macropores through which the gases diffuse before entering the microchannels of the carbon agglomerates) is more appropriate than the macrohomogeneous one (i.e. the active layer is considered as a homogeneous domain, in which the various transport media are simply superimposed to each other), as the former explains better the mechanism of diffusion of the reactants in the active layer.

1.3.3. Membrane–electrode assembly (MEA)

In order to interpret the cell potential versus current density behavior, all the processes occurring in the anode, cathode and in the proton conducting membrane must be
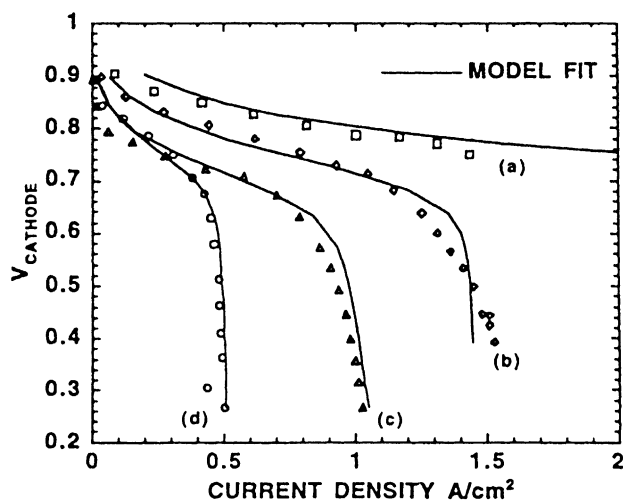

Fig. 6. Simultaneous fit to four cathode polarization curves for a 5 cm^2 PEMFC cell. Curve (a) is for 5 atm O$_2$, (b) for 5 atm air, (c) for a 2 atm O$_2$/ N$_2$ mixture with 13.5% O$_2$, and (d) for a 5 atm O$_2$/N$_2$ mixture with 5.2% O$_2$. From [38], with permission.

considered. Thus, MEA models couple the electrode model, described in the previous sub-section, to a model of the membrane sandwiched between the two electrodes. The latter problem is much more complex than that presented in the sub-section for modeling of the membrane since, under real fuel cell operating conditions, there is a water flux through the membrane which determines the electrolyte overpotential and the performance of the MEA (Fig. 7); in addition, the water content is not uniform along the thickness of the membrane, causing performance losses. Simulation studies of these phenomena have been carried out using different approaches; in all of those the membrane region was considered as a homogeneous domain under steady-state conditions. The first 'quantum jump' is found in the studies of Bernardi and Verbrugge [25,26,39]. Their treatment is based on the dilute solution theory (Nernst–Plank equation)

$$N_i = -z_i \frac{F}{RT} D_i c_i \nabla \Phi - D_i \nabla c_i + c_i \boldsymbol{v} \tag{8}$$

According to the above equation, a species dissolved in the fluid in the pore of a membrane can move by migration (under the effect of the electrical potential gradient), diffusion and convection; N_i represents the flux of the species i, D_i is the diffusion coefficient, z_i and c_i are the charge number and the concentration of the mobile species within the membrane, $\boldsymbol{v}$ the velocity and Φ the electrical potential. The equation above is coupled to the Schögl's equation, which provides a description of the fluid dynamics in the membrane pores

$$\boldsymbol{v} = \frac{k_\Phi}{\mu} z_f c_f F \nabla \Phi - \frac{k_p}{\mu} \nabla p \tag{9}$$

where k_Φ and k_p are the electrokinetic permeability and the membrane hydraulic permeability, respectively, and z_f and c_f
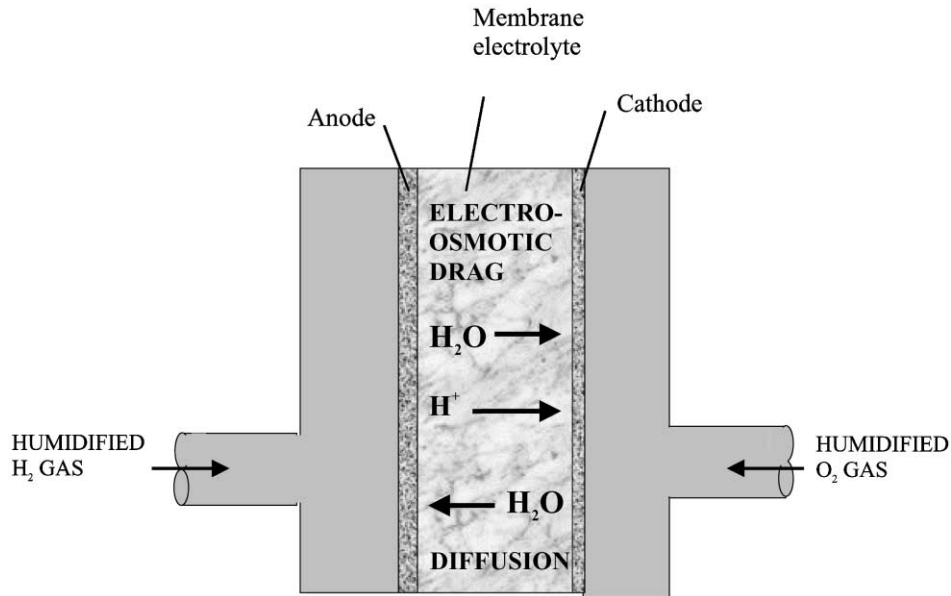
Fig. 7. Water transport phenomena in the polymeric electrolyte of the fuel cell.

represent the charge number and the concentration of the fixed species within the membrane. The above equation states that the electric potential and pressure gradients generate convection within the pores of the ion-exchange membrane. These equations are coupled to

  (i) the necessary current conservation condition:

$$\nabla \cdot i = 0 \tag{10}$$

 (ii) the steady-state material balance:

$$\nabla \cdot N_i = 0 \tag{11}$$

(iii) the equation of continuity for incompressible fluid flow:

$$\nabla \cdot v = 0 \tag{12}$$

(iv) the condition of electroneutrality within the membrane:

$$z_f c_f + \sum_i z_i c_i = 0 \tag{13}$$

As already mentioned, in this model the membrane and the reactant gases are assumed to be fully humidified. Thus, the water content of the membrane and the dehydration effects are not taken into account in evaluating the membrane overpotential; instead, the flux of water through the membrane plays a role. The results of the calculations of water velocity through the electrolyte are shown in Fig. 8 for different values of cell current density. In the case study, the cell is considered to be at a temperature of 80°C, with air and hydrogen at cathodic and anodic side, respectively; pressure is 5 and 3 atm at the cathodic and anodic side, respectively. In Fig. 8, the pressure driven flow is the most important effect at low current densities (100 mA/cm²), which causes a flux of water throughout the cell from the anodic to the

cathodic side, as evidenced by the negative value of water velocity at the cathode diffuser: under those conditions, even though water is produced by the electrochemical reaction, liquid water must be supplied at the outer face of the cathode (which can be done by humidifying the cathodic reactant gas at a temperature higher than the fuel cell temperature). The reverse situation occurs when the current density is 600 mA/cm²: under such a condition, the electro-osmotic
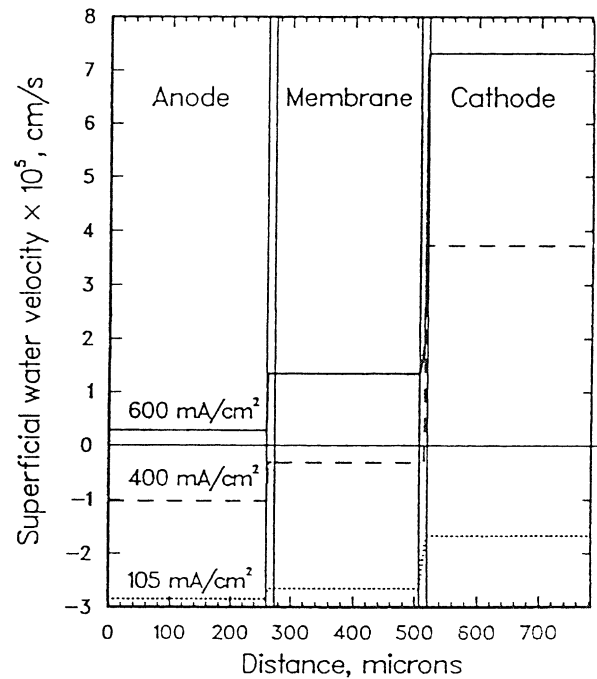

Fig. 8. Model calculations of superficial water velocity throughout the fuel cell for different values of current density. See text for operating conditions. From [26], with permission.

drag is the prevailing phenomenon, which causes the electrochemically produced water to generate a build-up of hydrostatic pressure sustained by the hydrophobic nature of the cathode backing. Thus, the anode, instead of the cathode, needs to be supplied with water in this case. The intermediate case (current density 400 mA/cm^2) shows the most interesting situation, where the water produced in the active catalyst layer flows out both sides of the fuel cell (about 75% of it flows out the cathode and the remaining flows out the anode). For this type of flow pattern, it may not be necessary to supply liquid water to the cell; this situation occurs approximately between 150 and 550 mA/cm^2. However, other authors [40] have observed experimentally that it is difficult to operate PEMFCs under such operating conditions and at a current density of 400 mA/cm^2 without external supply of water — at least to the anode — and suggest that the evaporative water losses from cell, which are not taken into account in the model, are responsible for the discrepancy between the model calculations and the experimental results.

The integration of the membrane and electrode models described above and in the previous sub-sections allows the evaluation of the cell potential versus current density (E versus i) plot of the MEA. Fig. 9 shows an evaluation [26] of the relative importance of the different overpotentials: cathodic losses are by far the most relevant dissipations, while anodic losses are almost negligible. The E versus i plot can be analyzed taking into consideration three regions: (i) at low current density, the behavior is semi-exponential, being determined by activation overpotentials in the cathode; (ii) the intermediate region is generally linear, in which the ohmic losses in the MEA play a mayor role and (iii) at high current density (not reported in Fig. 9), the limitations related to both water transport in the membrane and reactant transport in the cathode become the rate determining step of
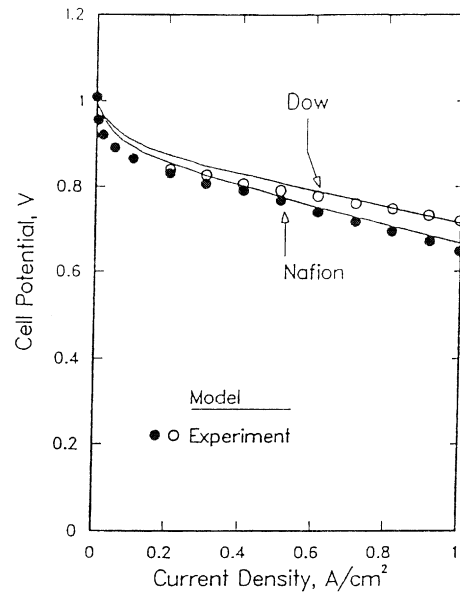

Fig. 10. Model and experimental results for cell potential as a function of current density for two types of membranes: a 5 mil thick Dow membrane and a 4 mil thick Nafion membrane. H$_2$/O$_2$ fuel cell, $T = 95°$C, anodic and cathodic pressures 4 and 5 atm, respectively. From [26], with permission.

the process (concentration overpotentials), causing a steep decrease in E. A testing of the model, using some experimental data, shows good agreement (Fig. 10).

While in this study the membrane was supposed to be fully hydrated under all the operating conditions, in another study [41] the effect of the water content of the membrane on the proton conductivity and finally on the polarization losses of the MEA have been analyzed. In this case, the water content of the membrane, which was considered not to be uniform along the thickness of the membrane, was determined by a local water balance, according to the equation

$$\chi \frac{I}{n_e F} = \zeta \lambda \frac{I}{n_e F} - \frac{\rho^{memb}}{M} D_\lambda \frac{\partial \lambda}{\partial z} \qquad (14)$$

where the term on the left-hand side is the net flux of water through the membrane (χ being the ratio between the net water flux through the membrane and the water produced by the electrochemical reaction), and the first and second terms on the right-hand side represent the electro-osmotic drag (water transport from the anodic to the cathodic side due to the solvated proton flow) and the water diffusion from high to low concentration regions (usually from the cathodic to the anodic side of the membrane, Fig. 7), respectively. ζ is the electro-osmotic drag coefficient, λ the local number of water molecules per fixed SO$_3^-$ charges in the membrane, ρ^{memb} the density of the dry membrane and D_λ the diffusion coefficient of water in the membrane pores, which is related to the local humidity content through the following experimental relationship:

$$D_\lambda = (\varphi_1 + \varphi_2\lambda + \varphi_3\lambda^2 + \varphi_4\lambda^3) \exp\left[\varphi_5\left(\frac{1}{\varphi_6} - \frac{1}{T}\right)\right] \qquad (15)$$
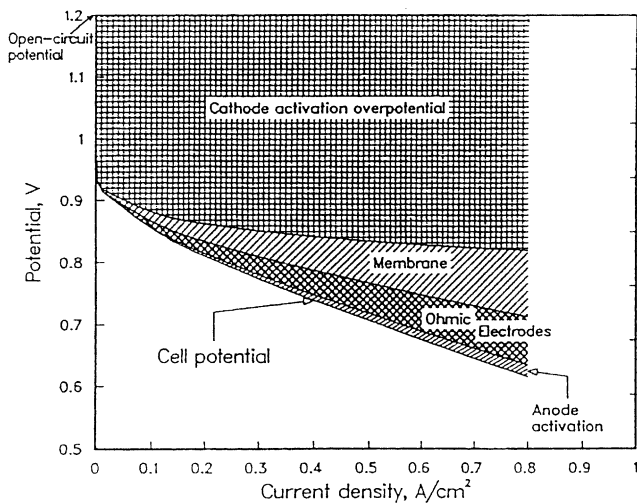

Fig. 9. Cell potential vs. current density characteristic curve of a typical PEM membrane–electrode assembly, with the nature and order of magnitude of the different overvoltages. From [26], with permission.

where T is the temperature and φ_1–φ_5 are phenomenological coefficients. The integration of the above equations, with the appropriate boundary conditions, leads to the evaluation of the net water flux through the membrane and of the profile of water content λ along the thickness of the membrane. In turn, the proton conductivity of the membrane is variable along the membrane thickness, and is a function of the local hydration λ

$$\sigma^{memb} = (\gamma_1\lambda - \gamma_2) \exp\left[\gamma_3\left(\frac{1}{\gamma_4} - \frac{1}{T}\right)\right] \qquad (16)$$

where γ_1–γ_4 are phenomenological coefficients evaluated through experimental measurements. Model results [41] (Fig. 11) show that the water content of the membrane is higher at the cathodic side than at the anodic side, and that severe dehydration can occur at the anodic side at high current densities, when the electro-osmotic water removal is fast and the back diffusion phenomenon is not efficient enough to re-equilibrate the humidity level. This results in a significant increase of the membrane resistance at high current densities, causing departures from linearity for the fuel cell E versus i plot (Fig. 12). An important remark that the authors make about their model is that, while the model does not predict the need to humidify the cathode feed stream at any appreciable current density, with real fuel cells based on Nafion 117 membranes the highest performance is obtained only with well-humidified cathodic flow streams. The authors suggest that the reason for this discrepancy is due again to significant evaporation effects (not included in the model), which cause an excessive water loss from the membrane and cannot be compensated by the water produced at the cathode. Moreover, another effect that the MEA models do not take into account is the accumulation of excess liquid water in the cathode, which could contribute to a high degree of hydration of the membrane but at the same time may lead to high resistances for diffusion of oxygen. A solution to compromise the two conflicting effects of excess liquid water at the cathode is still needed, and it is of fundamental importance for the optimized operation of PEMFCs.

1.3.4. Fuel cell

In general, physico-chemical variables, such as temperatures and gas compositions, are not uniform on the cell plane. An example is that, in some portions of the cell, water can be formed as a liquid and can condense in the back of the active layer, in the diffusion layer and/or in the substrate layer, as well as in the flow channels. Thus, additional mass transport problems could be encountered; in order to find solutions to these problems, mass transport phenomena must be evaluated not only across the MEA, but also in the planar directions; in-plane transport of energy and momentum is essential to complete the picture. In this case, the MEA model discussed above is used as a local kinetics subroutine of an overall fuel cell model that also includes macroscopic mass, energy and momentum balances.
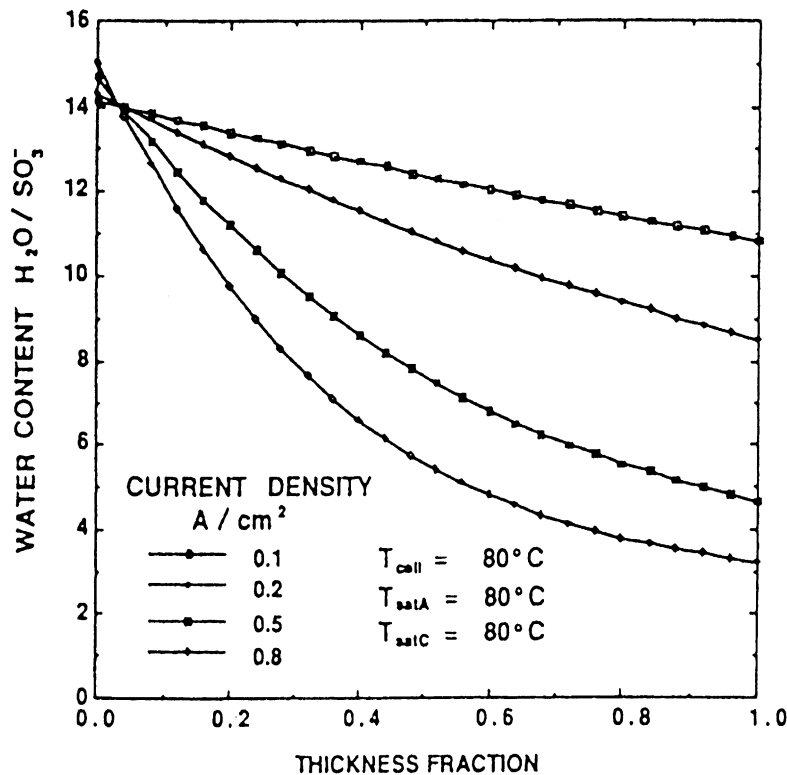

Fig. 11. Simulated water profiles in a H_2/air PEMFC, 80°C, 3 atm. Cathode and anode on the left- and right-hand side, respectively. From [41], with permission.
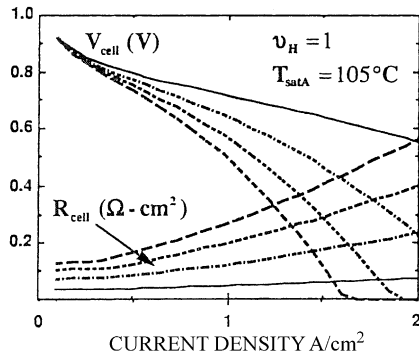
Fig. 12. Simulated cell voltage and membrane resistance vs. current density in a H_2/air PEMFC, 80°C, 3 atm. Membrane thickness: (—) 50 μm, (—·—·—) 100 μm, (- - -) 140 μm, (— — —) 175 μm. From [41], with permission.

Nguyen and coworkers [42,43] presented a two-dimensional model of this type; along the direction perpendicular to the cell plane the membrane water content was evaluated following an approach very similar to the one proposed by Springer et al. [41], as discussed in the previous sub-section. The second coordinate, x, was for the gas channel direction (which was considered to be the same at both the anodic and cathodic side). The basic mass and energy balances along the x-coordinate are represented by [42]

$$\frac{dM_i}{dx} = -hN_{i,y,k}(x) \tag{17}$$

$$\sum_i (M_i C_{p,i}) \frac{dT_k}{dx} = (H^v_{w,k} - H^l_{w,k}) \frac{dM^l_{w,k}}{dx}$$
$$+ Ua(T_s - T_k) \tag{18}$$

where M_i is the molar flow rate of the species i, h the channel width and $N_{i,y,k}$ the y-component molar flux of species i in k channel; $C_{p,i}$ the heat capacity of the gas i, T_k the gas temperature in the k channel, $H^v_{w,k}$ and $H^l_{w,k}$ are the enthalpy of water vapor and of liquid water, respectively, in k stream, U the heat transfer coefficient, a the heat transfer area per unit length, and T_s the solid temperature.

According to the mass balance (Eq. (17)), the number of moles of the species i changes along the channel length due to the normal flux into or out of the membrane; condensation and evaporation effects are considered through additional equations which are not reported here. The energy balances of the gases (Eq. (18)) include the heat transfer between the solid and gas phases and the latent heat associated with evaporation and condensation of water in the flow channels, and allow the evaluation of the gas temperature distribution. The energy balance of the solid is included only in a more sophisticated version of this model [43]. While momentum balances are neglected.

The results [42,43] show that as the reactants flow along the channels, the partial pressure of water in the anode gas and the water content of the membrane at the anodic side decreases due to the electro-osmotic water transport from anode to cathode; as a consequence, the membrane resistance increases along the channel direction. At the same time, due to the reactant consumption, the local thermodynamic potential for the electrochemical reaction decreases and so does the kinetics of the reaction; these are the reasons for the current density to decrease along the channel direction. The temperature distribution shows a maximum in the middle of the cell, due to the energy dissipations of the electrochemical reaction; temperatures at the edges of the fuel cell are lower due to the heat exchange with the surroundings at low temperature. The model has been used to demonstrate that counter-flow geometry is more efficient that co-flow [43] in terms of heat-exchange, allowing better voltage–current cell performance. Also, different humidification schemes have been studied [42,43], demonstrating the advantages of liquid water injection over the traditional water bubbling humidification. The benefits of applying high cathodic pressures [43] are due to an increase of counter-flow of water from the cathodic to the anodic side which helps in maintaining a high level of hydration throughout the membrane and accounts for the high proton conductivity and good electrochemical performance [43].

One of the difficulties with the theoretical treatment reported above is that there is no analytical solution when all types of rate limiting processes are present in the electrode and/or electrolyte. Thus, a semi-empirical equation has been proposed to fit the E versus i plot for single cells with H_2/O_2 or H_2/air reactants under different operating conditions of temperature and pressure (Fig. 13) [44]

$$E = E_0 - b\log(i) - Ri - m\exp(ni) \tag{19}$$

The second and third term of Eq. (19) represent the Tafel and the Ohm's laws, respectively, while the exponential part is related to the mass transfer limitations; however, the physico-chemical rationale for this expression has not been clarified on theoretical grounds yet as for the third term on the right-hand side of the equation. This approach is strongly different from the previous ones, which are fully predictive models based on physico-chemical description of the involved phenomena. However, using this equation for the multitude of available experimental data, a database of values of E_0, b, R, m, n could be set-up; in addition, Eq. (19) could provide the basis for the simulation of the more complex electrochemical cell stack and the PEMFC power plant in respect to performance characteristics, optimizing operating conditions and thermal and water management.

1.3.5. Stack and system

Until the present time, no detailed results of modeling analyses of the performance characteristics of the electrochemical cell stack and the PEMFC power plant have appeared in the literature. Such studies have been and are being conducted by the fuel cell developers and the results of their analysis is proprietary. Some studies on specific aspects, such as the flow distribution within the stacks [45], have been published. Indeed, in the case of large stacks there
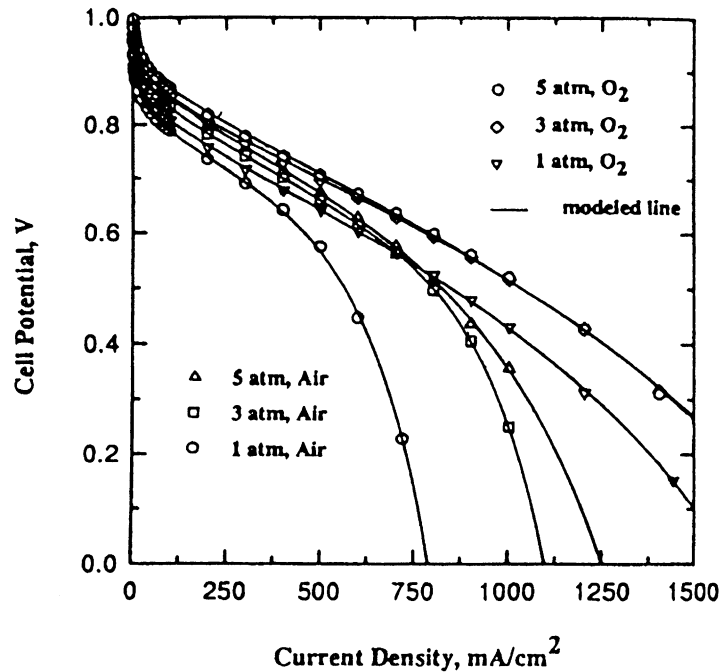
Fig. 13. Cell potential vs. current density plot in a PEMFC with Nafion 115 at 70°C. The figure shows the excellent agreement of the semi-empirical equation (Eq. (1)) (solid ones) with the experimental data. From [44], with permission.

is the risk that reactant starvation occurs in some of the cells, either due to channel blockages or non-uniform distribution of reactants caused by fluid-dynamics problems. In such a case, some cells may operate as electrolyzers leading to complete failure of the stack. The lower the ratio between pressure drop of the gases along the single cell channels and along the stack manifolds, the less uniform will be the feeding distribution between the various cells of the stack. Momentum balances for the stack manifolds, used to evaluate the pressure distribution along the manifolds [45], have been helpful in the design of channels and manifolds in order to choose a trade-off solution between the stack energy losses due to non-uniform reactant distribution among the cells and the cost for compression and recirculation of reactant gases.

Parametric modeling has been proposed for PEMFC stacks, based on the correlation (linear regression) of experimental data collected in a certain range of operating conditions [46]. The empirical model has demonstrated the ability to predict the experimental behavior of the stack much beyond that operational range [46]. These empirical models are also the basis for system simulations, which usually include the PEMFC stack model in a parametrized form [17,47]. The other components of the plant (i.e. fuel compressor, fuel processor, batteries, etc.) are modeled in the same simplified way, but still paying attention to the heat dissipation and heat transfer process. In fact, an efficient use of the waste heat is of major importance in order to find the most efficient plant configuration, which is one of the main aims of system modeling.

2. Quantum jumps in technology development and applications

2.1. First application of PEMFCs in NASA's Gemini Space Flights

PEMFCs found their first application at the beginning of the 1960s, in the NASA's Gemini Space Flights and this was indeed the first application for all types of fuel cells. In fact, NASA's space program, started in the late 1950s, gave birth to and stimulated the research, development and demonstration of all types of fuel cells for terrestrial application — power generation, transportation and portable power. In the Gemini flights, 1 kW PEMFCs provided auxiliary power requirements in the space vehicles and drinking water for the astronauts (Fig. 14). These power sources were designed
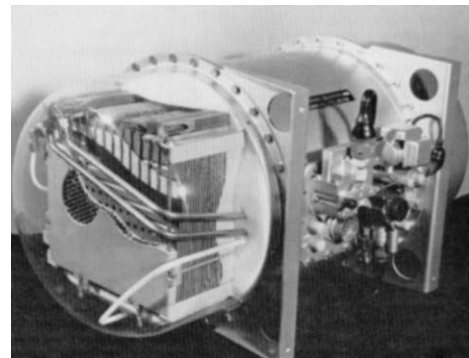

Fig. 14. GE 1 kW Gemini SPFC module. From [50], with permission.

and developed by the General Electric Company. The subsequent applications of the GE technology were the 350 W module for the Biosatellite spacecraft, the 3 kW module developed for a Navy high altitude balloon program, the regenerative fuel cell-electrolyzer breadboard hardware built for NASA in 1983.

2.2. NASA's other space projects

Since the late 1960s, the PEMFCs were displaced by alkaline fuel cell (AFC) power sources for NASA's Apollo and Space Shuttle flights. The main reason for the technology transfer for these applications were the higher attainable efficiency and the power density with the AFC than with the PEMFC technology during the starting phases of these programs. However, with the major strides in performance made by the PEMFCs since the late 1980s, there is renewed interest for the take-over of the PEMFC technology in NASA's space station and Mars programs. The rationale is that in these long duration flights, it will be essential to couple photovoltaic power systems with hydrogen energy storage systems and the proton exchange membrane technology for both power production and water electrolysis; this PEM technology is considerably more promising than the alkaline fuel cell and water electrolysis technologies in respect to efficiency, specific power, power density, specific energy and energy density. Further, another 'quantum jump' in the PEMFC technology is the demonstration of a highly efficient unitized regenerative unit, performing the fuel cell and electrolysis functions, which will be most beneficial.

2.3. Automobiles and buses

Interest in the application of fuel cells as power sources for electric vehicles started in the late 1970s, but received a major boost in the late 1980s and early 1990s, firstly because of the California Environmental Legislation to develop ultralow and zero emission vehicles, and secondly because of the Partnership for a New Generation of Vehicles (PNGV) program, initiated in the USA in 1993 to develop automobiles with three times the efficiency of the present 'conventional IC engine powered vehicles'. The fuel cell engine is the best substitute for an IC or diesel engine, because of its prospects for achieving higher efficiency (and hence lower fuel consuption) and being potentially zero-emission in an automobile. Further, the PEMFCs is the best choice among all different types of fuel cells, as (i) it operates at low temperatures (vital for a rapid start-up time), (ii) it contains the most innocuous electrolyte (a hydrated proton conducting plastic polymer), and (iii) exhibits the highest efficiencies and power densities. Two types of PEMFC on-board plants have been proposed, e.g. (i) stack coupled to an electric motor, (ii) stack coupled to an electric motor with back-up batteries (hybrid system). In the hybrid systems, batteries have the function of (i) recovering the energy lost during braking in start–stop cycles (city-type driving) and

(ii) providing the additional power for start-up, acceleration and hill climbing. The hybrid configuration is more advantageous than the single power source (fuel cell) configuration because of it being capable of providing higher power for the same specifications of the power source and reducing production costs. Several configurations have been proposed for both hybrid and non-hybrid cars — use of different types of batteries and of different ratios of fuel cells to battery power. However, none of these solutions predominates at the present time: the development of the PEMFC technology and of the fuel infrastructure will greatly influence tomorrow's choice. Up to now, the 'quantum jump' in on-board PEMFC applications was made in March 1998, when the first passengers boarded a fuel-cell bus in Chicago (Fig. 15). The bus was built in a program involving Chicago Transit Authority, British Columbia Transit and Ballard/Daimler Benz. Groups of three buses each have been delivered in Chicago and Vancouver, and they are currently in service, in a demonstration program aimed at collecting data for the design of the next generation of PEMFC buses. Each of the demonstration buses features 10 fuel cell stacks for an overall power of 200 kW; the fuel is gaseous hydrogen compressed at 300 bar and stored in seven tanks, and is sufficient for a 400 km range; the electric power generated by the fuel cells is transmitted to three-phase asynchronous ac electric motors with no back-up batteries being present in the system. Sixty passengers can be carried on-board, thanks to a partial optimization of the distribution of the components; the electric motors are located close to the wheels, the fuel cell modules at the rear of the bus (in the space that is for the diesel engine in the present buses), and both the cooling unit and the hydrogen tanks are on the roof. The bus described above is the third phase (demonstration fleets) of a program that started from a 93 kW/160-km bus in a proof-of-concept phase in 1993, and aimed for commercial production (announced for 2002) of a 200 kW fuel cell power plant and a 560 km range bus able to carry 75 passengers. Ballard has also developed fuel cells for automobile applications since 1989. A collaboration between Ballard and DaimlerChrysler, that has recently involved Ford as well, has given birth to the fuel cell powered electric cars (NECAR series): NECAR 2 and 3 vehicles have already been demonstrated, and their characteristics are presented in Table 1. The project is now in the fourth phase of development, focusing on NECAR 4 (Fig. 16, DaimlerChrysler/Ballard/Ford joint venture) [48]; the production of this vehicle is scheduled the year 2004 with an entry price around US$ 45,000. The vehicle (front-engine, front-wheel-drive, five-door sedan) will be able to carry five passengers, and will be based on two stacks of 160 fuel cells each, supplying an overall power of 70 kW at 340 A to an asynchronous ac electric motor. The fuel will be liquid hydrogen, stored in a 100 l tank, which will provide a 450 km range and will be utilized with an overall efficiency around 36%: the latter figure compares extremely favorably to the 24% achieved by the best diesels.
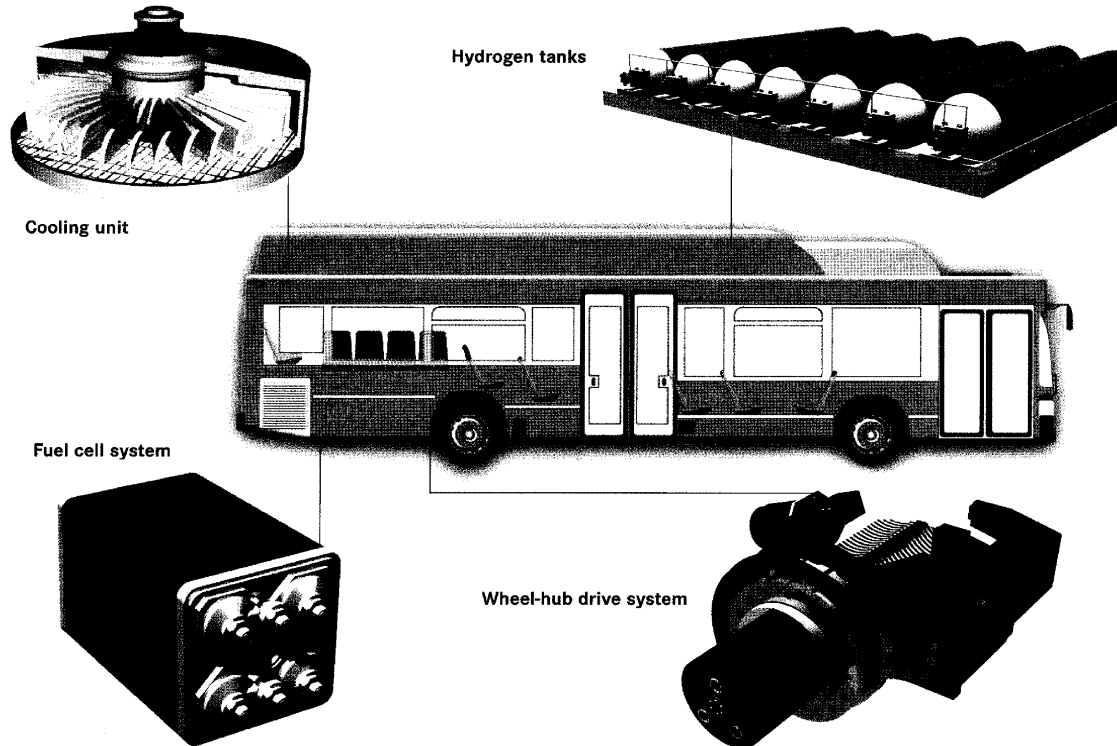
Fig. 15. Ballard–DaimlerChrysler's Nebus, featuring a 200 kW fuel cell motor; the fuel is gaseous hydrogen compressed at 300 bar, providing a 400 km range. From: http://www.ballard.com.

Other automobile manufacturers in the US, Japan and Europe have also entered the arena. In January 1998, General Motors had announced a concept for a fuel cell vehicle based on a modified version of its EV1 electric car, and Ford Motor Inc. is working on a fuel cell version of its P2000 vehicle. The Japanese and European fuel cell car projects have concentrated on hybrid concepts (Table 2). In Japan, Toyota is developing two fuel cell RAV4 mini sport-utility vehicles; one of the vehicles uses metal hydride storage and has a range of 250 km, and the other uses methanol steam, reformed on-board the vehicle, and has a range of 500 km. Mazda Motor Corp. presented its Demio vehicle in 1997, which has hydrogen stored in a metal hydride system, and uses ultra-capacitors for peak-power demands. Nissan, again in 1997, presented a concept of a fuel cell hybrid car with methanol reformer and lithium-ion batteries. In Europe, Renault and Volvo are leading the research and developments in this field, and have recently been followed by Fiat. Renault's Laguna (liquid hydrogen batteries, 500 km range)

and the vehicle jointly developed by Volvo, Johnson Mattey, The Netherlands Energy Research Foundation (car with methanol reforming and batteries) are both promoted by the European Economic Community (EEC).

2.4. Portable power sources — military and civilian

The PEMFC technology has a high potential for application in the field of portable power sources, where it may be able to compete with lithium ion or nickel/metal hydride batteries. One of the main advantages of fuel cells over batteries is the shorter charging time (a few minutes versus several hours); other features which make fuel cell interesting for portable applications are their high specific power and specific energy. Two companies, H-Power and Ballard Power Systems, are close to commercializing fuel cells for portable applications; the power levels range from 35 to 250 W and the fuel is hydrogen, which is provided from either a metal hydride cartridge or an external tank of

Table 1
Characteristics and performance parameters for DaimlerChrysler demonstration vehicles

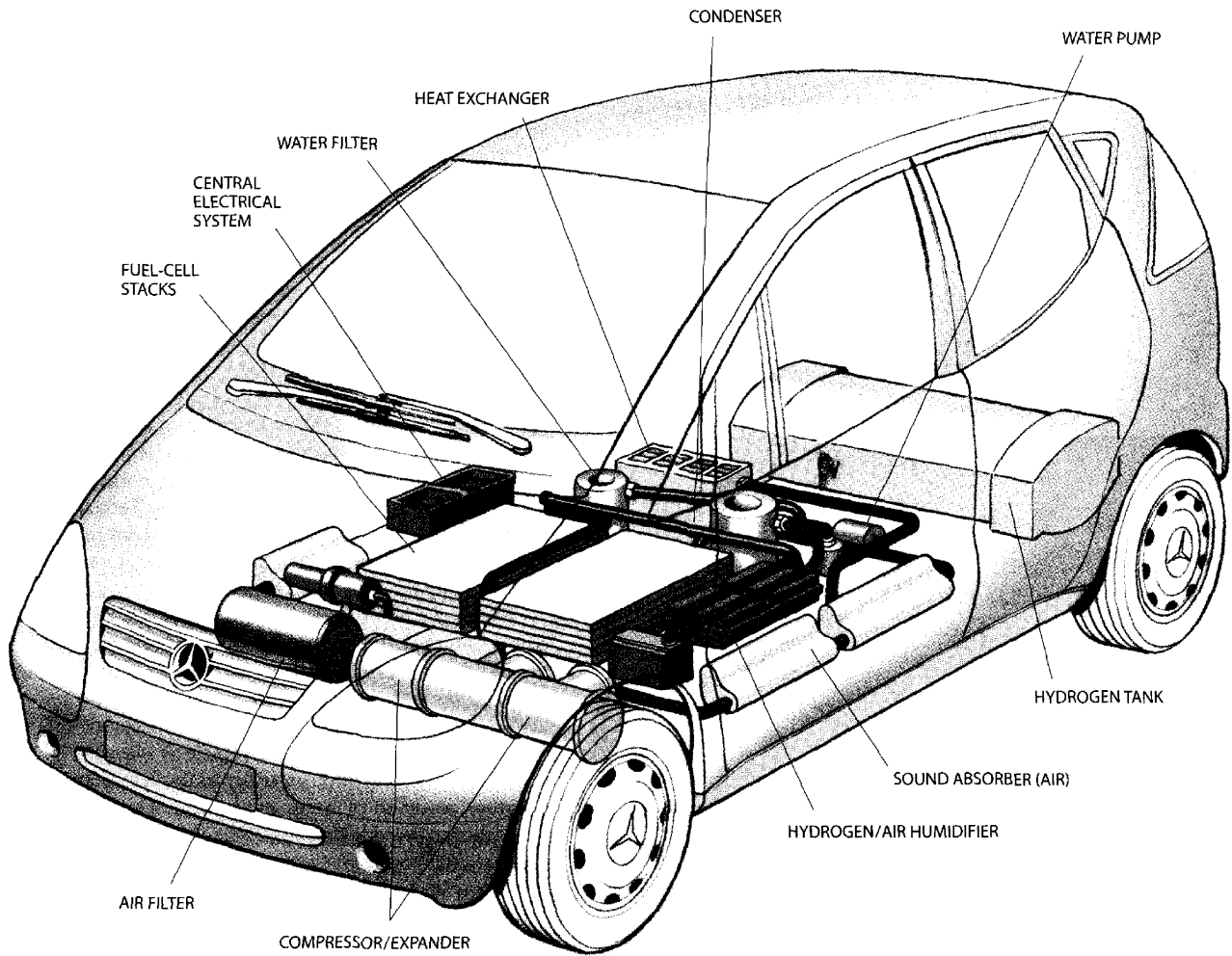| Vehicle name	Vehicle type	Year of demonstration	Fuel cell power (kW)	Fuel	Energy storage and capacity	Range (km)
Daimler NECAR 2	Van	1996	50	Compressed H_2	5 kg, 250 bar	250
Daimler NECAR 3	Compact car	1997	50	Methanol	38 l	400
Daimler NECAR 4	Compact car	1999	70	Liquid H_2	5 kg, $-250°C$	450

Fig. 16. Ballard–DaimlerChrysler's NECAR 4, featuring a 70 kW fuel cell motor, with fuel cells installed under the floor of the car. The fuel is liquid hydrogen, stored in a 100 l cryogenic tank, which provides a 450 km range and is utilized with an overall efficiency around 36%. From [48], with permission.

compressed hydrogen. Possible applications are video cameras, electric wheelchairs, portable-power briefcases, laptop computers, intelligent transportation systems (road signs, traffic lights, etc.) and military communications. The challenges to be overcome in order to compete with the available technologies for portable applications are (i) capability of operating at ambient temperature and pressure and using oxygen from air as the cathodic reactant, (ii) minimizing irreversible heat losses, in order to use air-cooling, and (iii) developing new water management techniques, in order to

use only fuel cell product water. If all of these challenges are overcome, the fuel cell will offer power and energy performance superior to those of batteries, in the range of 50–250 W; in addition to that, a longer lifetime is expected as well.

2.5. Power generation systems: residential and buildings

Previous speculations about fuel cell power plants for these applications are close to realization because of the

Table 2
Characteristics and performance parameters of demonstrated hybrid electric vehicles

Vehicle name	Year	Fuel	Storage	Fuel cell power (kW)	Auxiliary type	Auxiliary power (kW)	Range (km)	Vehicle type
Toyota RAV4	1996	Hydrogen	2 kg hydrides	25	Lead acid battery	25	250	SUV
Toyota RAV4	1997	Methanol	50 l	25	NiMH	25	500	SUV
Mazda Demio	1997	Hydrogen	1.3 kg hydrides	20	Ultra-capacitors	20	170	SUV
Renault Fever	1998	Hydrogen	8 kg cryogenic	30	NiMH	45	500	Wagon

'quantum jumps' in PEMFC technology. High temperature fuel cells are the first option for dispersed power generation and intermediate and large-size power plants (especially co-generation plants), also in combination with other existing conversion technologies. Solid oxide fuel cells (SOFCs), integrated with gas turbines of small size (<1 MW), are currently in the development phase. However, PEMFCs are attracting interest too, especially for small units that are expected to succeed in market niches where the benefit of extremely reliable, high quality power exceeds the cheaper cost of lower quality, grid-supplied power. In addition, environmental concerns are motivating the development of residential and building PEMFC plants for co-production of electricity and heat. It has been evaluated [49] that commercial buildings, rather than homes, are the segment of market where fuel cells have the best chance to make their entry, at an initial price higher than the target cost (e.g. US$ 800–1200/kW installed, whether at home or central station) where it is affordable. Development of such small units is in progress at a number of US companies, such as American Power Corp., Plug Power-General Electric Power Systems, Avista Laboratories and Northwest Power Systems. For example, the Plug Power-General Electric Power Systems Module (Fig. 17) is able to supply 7 kW continuously, and is able to support short-time peaks (i.e. 10 kW for 30 min and 15 kW for 0.5 s) assisted by back-up batteries, being charged during the periods when the power generated by the fuel cell exceeds the demand. This system has the size of a small refrigerator (volume around 1 m^3), and can be operated with natural gas, LPG or methanol. The package includes the fuel-processor, the fuel cell stack and the power-conditioning unit (batteries and inverter), which is the largest component. Commercialization is expected by the year 2001, and testing and demonstration is being made in 1999–2000. The price of the powerplant is expected to be in the range US$ 7500 to 10,000 when it is first introduced into the market, with the possibility of decreasing to US$ 3500 with mass production.

Ballard Power Generation Systems is also active in this field, and is developing a PEMFC stationary energy conversion plant of 250 kW power. The plant fits into a 50 m^3 volume, including fuel processor and power-conditioner units together with the fuel cell stacks. Methane, propane, hydrogen and anaerobic digester from waste water treatment facilities are being considered as the fuels. The first unit has been operated in 1997; a field trial is in progress in 1999–2000 and the first commercial unit is expected by the end of 2001.

3. Technological and economic challenges and 21st century perspectives

Even though the research efforts, made so far, have lead to a successful solution of many technological problems, bringing the PEMFC technology close to the era of commercialization, there are still some technological challenges: (i) choice of fuel (gasoline, methanol or hydrogen); (ii) efficient fuel processing, with reduction of weight, volume and CO residuals; (iii) finding anodic electrocatalysts tolerant to CO at levels of 100 ppm (with noble metal loading lower than 0.1 mg/cm^2 or less); (iv) inventing a cathodic electrocatalyst, to reduce the overpotential encountered at open circuit and to significantly enhance the exchange current density; (v) finding alternative proton conducting membranes with lower cost but same proton conductivity of the state-of-the-art perfluorosulfonic acid membranes; (vi) developing new proton conducting membranes not depending on water for high temperature operation between 150 and 200°C; (vii) manufacturing low-cost bipolar plates; (viii) developing an air compressor/turbine with improved performance and reduced size and cost; (ix) optimizing thermal and water management and (x) advancing DMFC technology to significantly increase the exchange current density for methanol oxidation, inhibit poisoning of the anode electrocatalyst by intermediates formed during methanol oxidation and minimizing cross-over of methanol from the anode to the cathode.

Cost reduction is vital to meet the goals set by the development programs, i.e. US$ 50/kW for the vehicle application and US$ 1000/kW for stationary power generation. The rapid progress in science and technology since the mid 1980s have raised the hopes for the cost goals to be achieved in the 21st century, leading to commercialization of PEMFCs for the transportation and power generation applications. The near-term perspectives (2000 A.D. and seq.) are the high prospects for developing portable power sources, in the range of 100 W to 1 kW for military and civilian applications. The intermediate-term projections (2010 A.D. and seq.) involve utilization of regenerative fuel cells for NASA's space stations and the Mars space flights, while PEMFCs are expected to play a role in the long-term scenario (2015 A.D. and seq.) as power sources for electric vehicles and powerplants for residential and commercial buildings.

Fig. 17. Plug Power-General Electric 7 kW system for residential applications. Volume: 1 m^3. From: http://www.ge.com.

Acknowledgements

References

[1] P.J. Schutz, in: R.E. White, A.J. Appleby (Eds.), Proceedings of the Symposium on Fuel Cells, PV 89-14, The Electrochemical Society Proceedings Series, Pennington, NJ, 1989, p. 87.

[2] D.L. Wood III, J.S. Yi, T.V. Nguyen, Electrochim. Acta 43 (1998) 3795.

[3] S. Miachon, P. Aldebert, J. Power Sources 56 (1995) 31.

[4] G. Faita, C. Mantegazza, US Patent No. 5482792 (9 January 1996).

[5] P.L. Hentall, J.B. Lakeman, G.O. Mepsted, P.L. Adcock, J.M. Moore, J. Power Sources 80 (1999) 235.

[6] R. Hornung, G. Kappelt, J. Power Sources 72 (1998) 20.

[7] E.A. Ticianelli, C.R. Derouin, A. Redondo, S. Srinivasan, J. Electrochem. Soc. 135 (1998) 2209.

[8] T. Nguyen, J. Hedstrom, N. Vanderborgh, in: R.E. White, A.J. Appleby (Eds.), Proceedings of the Symposium on Fuel Cells, PV 89-14, The Electrochemical Society Proceedings Series, Pennington, NJ, 1989, p. 39.

[9] M. Watanabe, Y. Satoh, C. Shimura, J. Electrochem. Soc. 140 (1993) 3190.

[10] H.P. Dhar, US Patent No. 5242764 (7 September 1993).

[11] M. Watanabe, H. Uchida, M. Emori, J. Electrochem. Soc. 145 (1998) 1137.

[12] D.P. Wilkinson, H.H. Voss, K. Prater, J. Power Sources 49 (1994) 117.

[13] H.H. Voss, D.P. Wilkinson, P.G. Pickup, M.C. Johnson, V. Basura, Electrochim. Acta 40 (1995) 321.

[14] R. Mosdale, S. Srinivasan, Electrochim. Acta 40 (1995) 413.

[15] K.B. Prater, Journal of Power Sources 51 (1994) 129.

[16] C.Y. Chow, B. Wozniczka, J.K.K. Chan, US Patent No. 5804326 (8 September 1998).

[17] J.M. Ogden, M.M. Steinbugler, T.G. Kreutz, J. Power Sources 79 (1999) 143.

[18] S.T. Naumann, C. Myren, J. Power Sources 56 (1995) 45.

[19] W.P. Teagan, J. Bentley, B. Barnett, J. Power Sources 71 (1998) 80.

[20] N. Edwards, S.R. Ellis, J.C. Frost, S.E. Golunski, A.N.J. van Keulen, N.G. Lindewald, J.G. Reinkingh, J. Power Sources 71 (1998) 23.

[21] K. Ledjeff-Hey, V. Formanski, T. Kalk, J. Roes, J. Power Sources 71 (1998) 199.

[22] T.D. Gierke, W.Y. Hsu, in: A. Eisenberg, H.L. Yeager (Eds.), Perfluorinated Ionomer Membranes, ACS Symposium Series No. 180, American Chemical Society, Washington, DC, 1982, p. 283.

[23] T. Okada, G. Xie, O. Gorseth, S. Kjelstrup, N. Nakamura, T. Arimura, Electrochim. Acta 43 (1998) 3741.

[24] M. Eikerling, A.A. Kornyshev, U. Stimming, J. Phys. Chem. B 101 (1997) 10807.

[25] D.M. Bernardi, M.W. Verbrugge, AIChE J. 37 (1991) 1151.

[26] D.M. Bernardi, M.W. Verbrugge, J. Electrochem. Soc. 139 (1992) 2477.

[27] J.-T. Wang, R.F. Savinell, Electrochim. Acta 37 (1992) 2737.

[28] Y.W. Rho, S. Srinivasan, Y.T. Kho, J. Electrochem. Soc. 141 (1994) 2089.

[29] F. Gloaguen, F. Andolfatto, R. Durand, P. Ozil, J. Appl. Electrochem. 24 (1994) 863.

[30] E.A. Ticianelli, J. Electroanal. Chem. 387 (1995) 1.

[31] K. Broka, P. Ekdunge, J. Appl. Electrochem. 27 (1997) 281.

[32] F. Gloaguen, R. Durand, J. Appl. Electrochem. 27 (1997) 1029.

[33] D. Bevers, M. Wöhr, K. Yasuda, K. Oguro, J. Appl. Electrochem. 27 (1997) 1254.

[34] F. Gloaguen, P. Convert, S. Gamburzev, O.A. Velev, S. Srinivasan, Electrochim. Acta 43 (1998) 3767.

[35] M.L. Perry, J. Newman, E.J. Cairns, J. Electrochem. Soc. 145 (1998) 5.

[36] M. Eikerling, A.A Kornyshev, J. Electroanal. Chem. 453 (1998) 89.

[37] C. Marr, X. Li, J. Power Sources 77 (1999) 17.

[38] T.E. Springer, M.S. Wilson, S. Gottsfeld, J. Electrochem. Soc. 140 (1993) 3513.

[39] M.W. Verbrugge, E.W. Scheider, R.S. Cornell, R.F. Hill, J. Electrochem. Soc. 139 (1992) 3421.

[40] S. Gottesfeld, T.A. Zawodzinski, in: R.C. Alkire, H. Gerischer, D.M. Kolb, C.W. Tobias (Eds.), Advances in Electrochemical Science and Engineering, Vol. 5, Wiley-VCH, Weinheim, Germany, 1997, p. 195.

[41] T.E. Springer, T.A. Zawodzinski, S. Gottesfeld, J. Electrochem. Soc. 138 (1991) 2334.

[42] T.V. Nguyen, R.E. White, J. Electrochem. Soc. 140 (1993) 2178.

[43] J.S. Yi, T.V. Nguyen, J. Electrochem. Soc. 145 (1998) 1149.

[44] J. Kim, S.M. Srinivasan, C.E. Chamberlin, J. Electrochem. Soc. 142 (1995) 2670.

[45] D. Thirumalai, R.E. White, J. Electrochem. Soc. 144 (1997) 1717.

[46] J.C. Amphlett, R.M. Baumert, R.F. Mann, B.A. Peppley, P.R. Roberge, A. Rodrigues, J. Power Sources 49 (1994) 349.

[47] J.C. Amphlett, R.F. Mann, B.A. Peppley, P.R. Roberge, A. Rodrigues, J.P. Salvador, J. Power Sources 71 (1998) 179.

[48] A.J. Appleby, Sci. Am. 281 (1999) 74.

[49] R.H. Wolk, IEEE Spectrum 36 (1999) 45.

[50] D.S. Watkins, in: L.J.M.J. Blomen, M.N. Mugerwa (Eds.), Fuel Cell Systems, Plenum Press, New York, 1993, p. 493.